



In-beam gamma rays of CSNS Back-n characterized by black resonance filter

Jin-Cheng Wang¹ · Jie Ren¹ · Wei Jiang^{2,3} · Xi-Chao Ruan¹ · Ying-Yi Liu¹ · Hao-Lan Yang¹ · Kuo-Zhi Xu¹ · Xin-Yi Pan¹ · Qi Sun¹ · Jie Bao¹ · Han-Xiong Huang¹ · Hao-Fan Bai⁴ · Jiang-Bo Bai⁵ · Ping Cao^{6,7} · Qi-Ping Chen⁸ · Yong-Hao Chen^{2,3} · Wen-Hao Duan^{6,9} · An-Chuan Fan¹⁰ · Rui-Rui Fan^{2,3,11} · Chang-Qing Feng^{6,9} · Min-Hao Gu^{2,11} · Chang-Cai Han¹² · Zi-Jie Han⁸ · Guo-Zhu He¹ · Yong-Cheng He^{2,3} · Yang Hong^{2,3,13} · Yi-Wei Hu⁴ · Zhi-Jie Jiang^{6,9} · Ling Kang^{2,3} · Chang-Lin Lan¹⁴ · Bo Li^{2,3} · Feng Li^{6,9} · Qiang Li^{2,3} · Xiao Li^{2,3} · Yang Li^{2,3} · Jie Liu⁴ · Rong Liu⁸ · Shu-Bin Liu^{6,9} · Yi-Na Liu¹ · Guang-Yuan Luan¹ · Chang-Jun Ning^{2,3} · Yi-Jia Qiu^{2,3} · Wen-Kai Ren⁴ · Zhi-Zhou Ren⁸ · Zhao-Hui Song¹² · Kang Sun^{2,3,13} · Zhi-Xin Tan^{2,3} · Jing-Yu Tang^{6,7} · Sheng-Da Tang^{2,3} · Li-Jiao Wang^{2,3,13} · Peng-Cheng Wang^{2,3} · Zhao-Hui Wang¹ · Zhong-Wei Wen⁸ · Xiao-Guang Wu¹ · Xuan Wu^{2,3} · Ze-Peng Wu⁴ · Cong Xia⁴ · Li-Kun Xie¹⁵ · Han Yi^{2,3} · Tao Yu¹⁵ · Yong-Ji Yu^{2,3} · Guo-Hui Zhang⁴ · Hang-Chang Zhang² · Qi-Wei Zhang¹ · Xian-Peng Zhang¹² · Yu-Liang Zhang^{2,3} · Zhi-Yong Zhang^{6,9} · Mao-Yuan Zhao^{6,9} · Zhi-Hao Zhou^{2,3,13} · Ke-Jun Zhu^{2,11,13} · Chong Zou¹

Received: 16 March 2024 / Revised: 21 June 2024 / Accepted: 26 June 2024 / Published online: 18 September 2024

© The Author(s), under exclusive licence to China Science Publishing & Media Ltd. (Science Press), Shanghai Institute of Applied Physics, the Chinese Academy of Sciences, Chinese Nuclear Society 2024

Abstract

The back-streaming white-neutron beamline (Back-n) of the China Spallation Neutron Source is an essential neutron-research platform built for the study of nuclear data, neutron physics, and neutron applications. Many types of cross-sectional neutron-reaction measurements have been performed at Back-n since early 2018. These measurements have shown that a significant number of gamma rays can be transmitted to the experimental stations of Back-n along with the neutron beam. These gamma rays, commonly referred to as in-beam gamma rays, can induce a non-negligible experimental background in neutron-reaction measurements. Studying the characteristics of in-beam gamma rays is important for understanding the experimental background. However, measuring in-beam gamma rays is challenging because most gamma-ray detectors are sensitive to neutrons; thus, discriminating between neutron-induced signals and those from in-beam gamma rays is difficult. In this study, we propose the use of the black resonance filter method and a CeBr₃ scintillation detector to measure the characteristics of the in-beam gamma rays of Back-n. Four types of black resonance filters, ¹⁸¹Ta, ⁵⁹Co, ^{nat}Ag, and ^{nat}Cd, were used in this measurement. The time-of-flight (TOF) technique was used to select the detector signals remaining in the absorption region of the TOF spectra, which were mainly induced by in-beam gamma rays. The energy distribution and flux of the in-beam gamma rays of Back-n were determined by analyzing the deposited energy spectra of the CeBr₃ scintillation detector and using Monte Carlo simulations. Based on the results of this study, the background contributions from in-beam gamma rays in neutron-reaction measurements at Back-n can be reasonably evaluated, which is beneficial for enhancing both the experimental methodology and data analysis.

Keywords In-beam gamma rays · Back-n · CeBr₃ scintillator · Black filter resonance technique

1 Introduction

The back-streaming white-neutron beamline of the China Spallation Neutron Source (CSNS) [1–6], known as Back-n, has served as a white-neutron facility for nuclear data measurements and neutron physics research since it became

This work was supported by the Youth Talent Program of China National Nuclear Corporation, the Continuous-Support Basic Scientific Research Project (BJ010261223282), the National Natural Science Foundation of China (No.11790321), and the Research and development project of China National Nuclear Corporation.

Extended author information available on the last page of the article

operational in early 2018 [7–12]. The layout of Back-n is shown in Fig. 1.

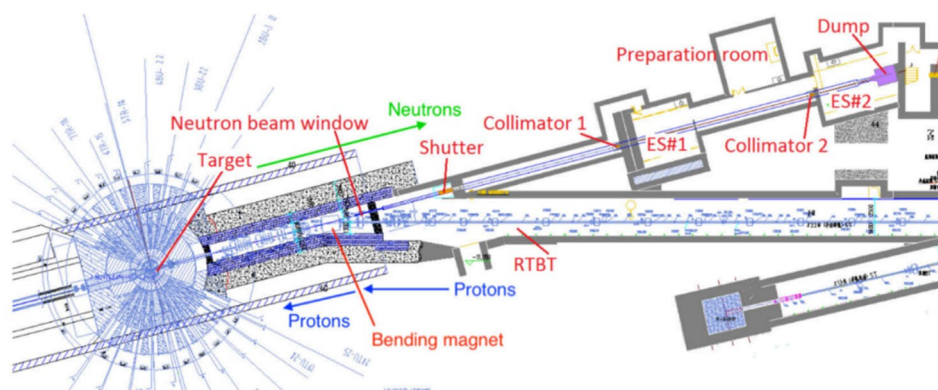
At CSNS, neutrons are generated by bombarding a proton beam with an energy of 1.6 GeV and a pulse-repetition rate of 25 Hz onto a spallation target made of tungsten. Before the incident proton beam hits the spallation target, it is deflected by 15 degrees by a bending magnet specifically designed for this purpose. Consequently, the neutron beamline of the Back-n was built in the 180-degree direction without any conflict with the proton-beam transfer line. Two experimental stations are located along the neutron beamline: The near station (ES#1) is approximately 56 m away from the spallation target, and the far station (ES#2) is approximately 20 m further than ES#1. At Back-n, different neutron-beam profiles can be obtained by changing the shape or size of the neutron collimators. Three collimators are located at ~ 24 , ~ 50 , and ~ 70 m away from the spallation target. The first collimator is also used as a beam shutter.

Several types of nuclear data have been measured at Back-n in recent years, including the neutron total cross section [13], radiative neutron-capture cross section [14–25], fission cross section [26, 27], neutron-induced charged-particle emission cross section [28, 29], and inelastic scattering cross section. However, the experimental background induced by gamma rays was non-negligible in many Back-n measurements, particularly when the detectors were sensitive to both neutrons and gamma rays. Based on recent research [14, 15], gamma rays generated in the spallation target can be transmitted to the experimental station along with the neutron beam. These gamma rays are known as in-beam gamma rays. Back-n has two main types of in-beam gamma rays. One type is generated by the spallation process, called γ -flash. These are composed of prompt gamma rays produced by spallation reactions and arrive at the experimental station within 300 ns after the proton beam hits the spallation target. The other type of in-beam gamma ray usually arrives at the experimental station later than the γ -flash and is caused by neutron reactions in the spallation target,

moderators, and structural materials. These gamma rays are called delayed in-beam gamma rays because they can last for more than 2 ms after the γ -flash. At Back-n, many types of nuclear data measurements are influenced by in-beam gamma rays. Taking the neutron radiative capture cross-section measurement as an example, the background caused by in-beam gamma rays is the main component of the experimental background in the neutron-energy region above 200 eV [14–23]. Therefore, determining the characteristics of the delayed in-beam gamma rays, such as energy distribution and time structure, can improve nuclear data measurements at Back-n. The energy distribution and time structure of the in-beam gamma rays were simulated in Ref. [14]. In addition, the time structure of in-beam gamma rays was evaluated using a lead (^{nat}Pb) sample [14–25] to capture the cross sections. However, the energy distribution and flux of in-beam gamma rays have not yet been measured for several reasons. First, in-beam gamma rays and those gamma rays produced by neutron-induced nuclear reactions are difficult to distinguish in-beam measurement experiments. Second, most gamma-ray detectors are also sensitive to neutrons, and separating the signals owing to gamma rays and neutrons is difficult. Third, detectors and electronic circuits can be damaged by the γ -flash and fast neutrons when the detectors are located in the neutron beam.

In this study, we propose a method using a CeBr_3 scintillation detector and the black resonance filter method [30] to determine the energy distribution and flux of gamma rays in the Back-n neutron beam. The black resonance filter method assists with absorbing neutrons at certain energies, which are determined using the time-of-flight (TOF) technique. Thus, within these absorption-energy regions, the in-beam gamma rays can be measured using the CeBr_3 scintillation detector without being affected by neutrons. The energy distribution of the in-beam rays is verified, and the flux is calculated by analyzing the deposition energy spectrum of the CeBr_3 scintillation detector and comparing it with Monte Carlo simulation results.

Fig. 1 (Color online) Layout of the Back-n beamline at CSNS



2 Methods

The black resonance filter method is effective for absorbing neutrons at certain energies without significantly altering the source neutron beam. Filters are employed to achieve a negligible transmission of neutrons at certain energies corresponding to a few strong resonances. Furthermore, the remaining events in the resonance region are not influenced by neutrons and represent in-beam gamma rays. In this study, the TOF method was used to determine the resonance energy of neutrons (E_n) via the following relation:

$$E_n = \frac{1}{2} m_n \left(\frac{L}{t_n} \right)^2, \quad (1)$$

where m_n denotes the neutron mass, L is the flight path, and t_n is the neutron flight time. At Back-n, t_n is determined as

$$t_n = (t_{\text{det}} - t_\gamma) + \frac{L}{c}, \quad (2)$$

where t_{det} is the time at which the detector responds to neutrons or γ rays, t_γ is the time at which the γ -flash arrives at the detector, and c is the speed of light.

Materials with strong resonances can be used as black resonance filters. By placing these filters in the neutron beamline, the neutrons are almost completely absorbed, allowing very few neutrons to reach the detector in the resonance energy regions. Therefore, the residual signals of the detector in the absorption region are considered to be mainly induced by the in-beam gamma rays. The advantage of using materials with strong resonances is that they enable a thin filter, which can reduce the attenuation of gamma rays in the beam. However, to achieve reasonable statistical precision, relatively thick filters must be used in practice. To determine the best absorption regions, the Geant4 toolkit [31] was used to simulate the transmission rate of the filters used in Back-n. In this simulation, the energy of the neutron beam was sampled according to the energy distribution of Back-n [8], and a virtual neutron detector was set up approximately 76 m away from the neutron source. The flight time required for the neutrons to pass through the filters and arrive at the detector was simulated. Five filters were used at Back-n, including a silver ($^{\text{nat}}\text{Ag}$) filter with a thickness of 0.4 mm, two cobalt (^{59}Co) filters with thicknesses of 0.4 mm and 1.0 mm, a 1.0-mm-thick tantalum (^{181}Ta) filter, and a 1.0-mm-thick natural cadmium ($^{\text{nat}}\text{Cd}$) filter. The simulated neutron TOF spectra, with and without the filter, are shown in Fig. 2. The dips absorbed by $^{\text{nat}}\text{Ag}$ (5.19 eV), ^{59}Co (132 eV and 5.016 keV), and ^{181}Ta (4.28 eV and 10.34 eV) can be clearly observed in the TOF spectrum of Fig. 2a. Based on the neutron-transmission rate in Fig. 2b, almost no neutrons were observed in the TOF regions near $\sim 85 \mu\text{s}$, $\sim 480 \mu\text{s}$, and $\sim 2.8 \text{ms}$, when the filters were online. Based on the

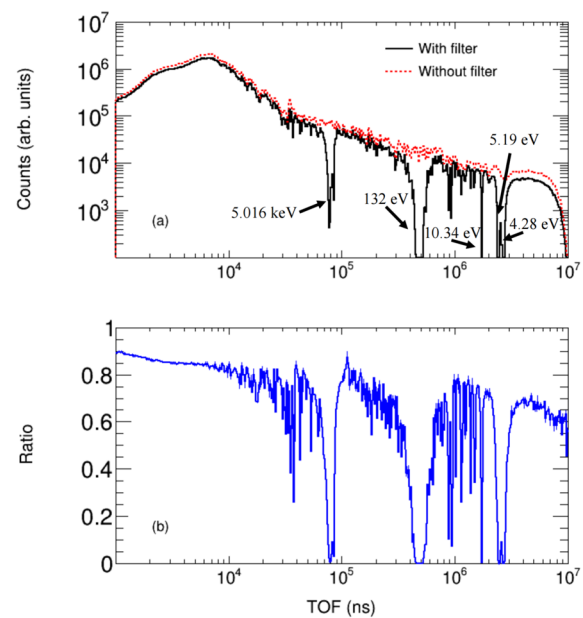


Fig. 2 (Color online) Simulated neutron TOF spectra at Back-n. **(a)** Neutron TOF spectrum with the filters online (the black solid line), and neutron TOF spectrum with the filters offline (the red dashed line); **(b)** neutron-transmission rate of the filters at Back-n

time distribution of the in-beam gamma rays measured in Ref. [14], very few in-beam gamma rays exist in the TOF region above 2.0 ms. Therefore, the absorption region near $\sim 2.8 \text{ms}$ is unsuitable for measuring in-beam gamma rays at Back-n. The transmission rate in the $480 \mu\text{s}$ TOF region was lower than that in the $85 \mu\text{s}$ TOF region, indicating that the neutrons were more fully absorbed in the $480 \mu\text{s}$ TOF region. Finally, the TOF region around $480 \mu\text{s}$ was chosen to measure the in-beam gamma rays in this study.

3 Experimental setup

The present measurement was performed at ES#2 of Back-n, with the CSNS operating in the two-bunch mode at a power of 140 kW. Figure 3 shows the layout of the experimental setup.

A CeBr_3 scintillation detector was used to measure the in-beam gamma rays located at the center of the neutron beamline, $\sim 76 \text{m}$ away from the spallation target. The CeBr_3 scintillator is used as a γ -ray detector in this study based on several reasons. First, the time response of the CeBr_3 scintillator to γ rays is less than a few tens of nanoseconds [32, 33], which is suitable for measurements using the TOF method. Second, the energy resolution of the CeBr_3 scintillator is better than that of commonly used gamma-ray scintillators such as $\text{NaI}(\text{TI})$ and BGO . Third, the intrinsic activity of the CeBr_3 scintillator is considerably lower than that of a

Fig. 3 Layout of the experimental setup

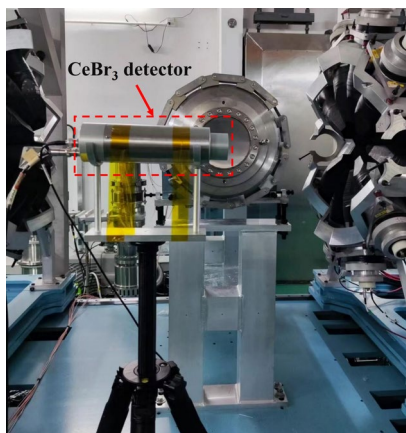
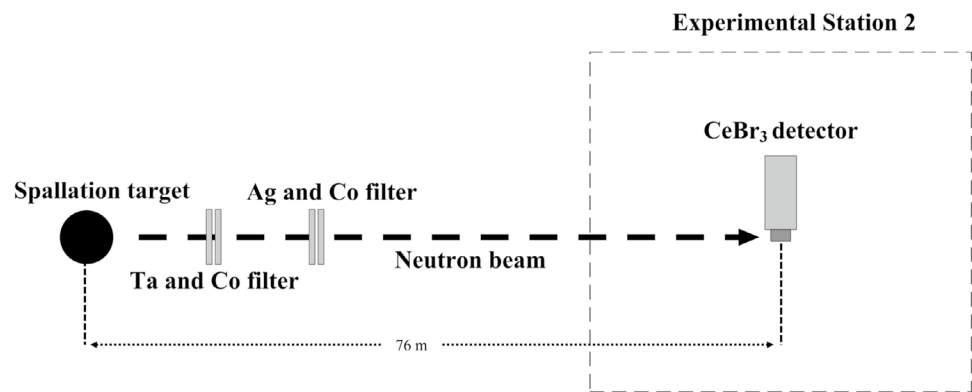


Fig. 4 (Color online) CeBr₃ detector at Back-n

LaBr₃ scintillator with the same volume. Finally, most of the γ rays emitted by Ce and Br after neutron activation are less than 1.5 MeV, indicating that the in-beam gamma rays above 1.5 MeV are rarely affected by the activation γ rays. The CeBr₃ scintillator used in this study had dimensions of $\Phi 38 \text{ mm} \times 38 \text{ mm}$ and was manufactured by SCIONIX Holland B.V, as shown in Fig. 4.

A photomultiplier tube (PMT; R13089, Hamamatsu, Japan) was coupled to the CeBr₃ scintillator to receive the scintillation light. The CeBr₃ scintillation detector was placed perpendicular to the direction of the neutron beam, which reduces damage to the PMT owing to γ -flash and high-energy neutrons. The signals from the anode of the CeBr₃ detector were transmitted directly to a digitizer (DT5730B, CAEN SpA, Italy). In addition, the pickup signal (T_0) from the pulsed proton beam was sent to the digitizer as the trigger for data acquisition.

The energy response of the CeBr₃ scintillation detector to gamma rays was calibrated using four radioactive sources: ²²Na, ⁶⁰Co, ¹³³Ba, and ¹³⁷Cs. The relationship between the deposited energy of the gamma rays and charge integral value of the digitized signal was calibrated

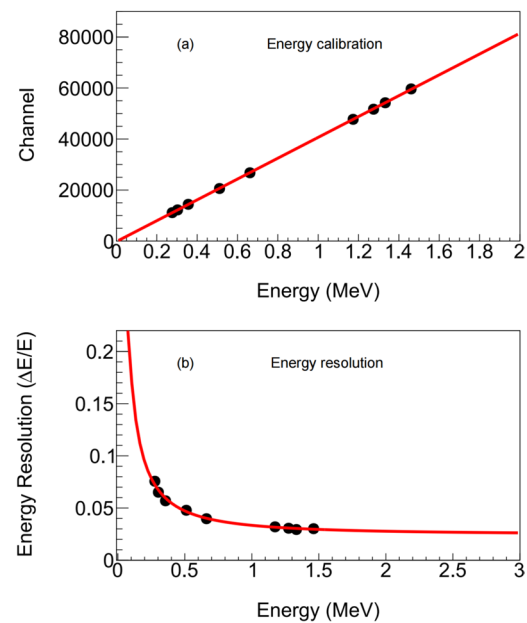


Fig. 5 (Color online) Energy calibration and energy resolution of the CeBr₃ detector. (a) Energy calibration. (b) Energy resolution

at energies of 0.276 MeV, 0.302 MeV, 0.356 MeV, 0.511 MeV, 0.662 MeV, 1.173 MeV, 1.275 MeV, and 1.332 MeV. Based on the calibration results shown in Fig. 5a, the charge integral value of the digitized signal exhibited good linearity with respect to the energy of the gamma rays. In addition, the energy resolution of the CeBr₃ scintillation detector was determined using the same measurements. As shown in Fig. 5b, the energy resolution of the detector was 4.0% at 662 keV.

In the present measurement, ¹⁸¹Ta and ⁵⁹Co filters, both 1.0 mm thick, were placed at a distance of approximately 26 m from the spallation target. A 0.4-mm-thick ⁵⁹Co filter and 0.4-mm-thick ^{nat}Ag filter were installed in the beam window chamber of Back-n. Additionally, a 1-mm-thick cadmium (^{nat}Cd) filter was installed in the beam window chamber to absorb neutrons with energies below 0.3 eV and

avoid overlap between consecutive neutron-beam pulses. The filter characteristics are shown in Table 1.

The aperture of the collimator was changed during this measurement to study the flux of the in-beam gamma rays with different collimator assignments. Three types of collimator assignments were measured in this study: 3 – 15 – 40 mm, 12 – 15 – 40 mm, and 50 – 15 – 40 mm, where 3 mm, 12 mm, and 50 mm correspond to the apertures of the neutron-beam shutter. The values 15 mm and 40 mm correspond to the apertures of collimators 1 and 2, respectively, which did not change in this measurement. To normalize the measurement results between the different collimator assignments, the intensity of the proton beam was recorded using the accelerator operating system of CSNS.

4 Data analysis

4.1 TOF spectrum

Signals from the CeBr₃ scintillation detector were digitized and recorded using a digitizer for offline analysis. Owing to its 14-bit resolution and 500 MS/s sampling rate, the digitized waveforms retained most of the characteristics of the original signals, such as amplitude, charge, and time. A typical waveform of the CeBr₃ scintillation detector is shown in Fig. 6 (black solid line). The rise time of this waveform is ~ 17 ns, and the full width is ~ 120 ns. The ADC channel of the ordinate in Fig. 6 represents the amplitude, with one channel representing approximately 0.122 mV. In this study, the charge integral value of the waveform was used to represent the deposited energy of the gamma rays in the CeBr₃ scintillator, which was calibrated using gamma-ray sources, as mentioned above. In the present waveform processing, the fast-filter (FF) and constant fraction discriminator (CFD) methods were used to handle the pileup signals and obtain good timing accuracy. The waveforms after FF and CFD are indicated by the red dashed and blue dotted lines in Fig. 6, respectively. The zero-crossing point of the CFD waveform was used as the signal time in the data analysis routine.

After waveform processing, the response time (T_{det}) was determined, and the TOF of the CeBr₃ detector was

Table 1 Characteristics of the filters

Sample	Shape	Dimensions (mm)	Thickness (mm)	Purity (%)
¹⁸¹ Ta	square	100.0	1.0	99.50
⁵⁹ Co	square	100.0	1.0	99.95
^{nat} Ag	circular	80.0	0.4	99.95
⁵⁹ Co	circular	80.0	0.4	99.95
^{nat} Cd	circular	80.0	1.0	99.95

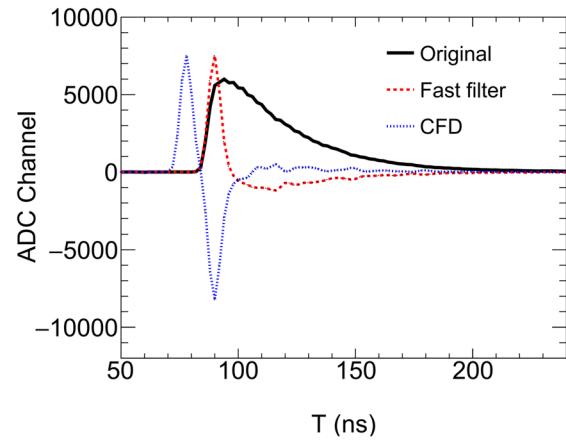


Fig. 6 (Color online) Original signal of the CeBr₃ detector and its derivative. The black solid line is the original waveform signal, the red dashed line is the waveform for fast filtering, and the blue dotted line represents the waveform of the CFD

calculated using Eq. (2). The experimental TOF spectra with the 3 – 15 – 40 mm collimator assignment are shown in Fig. 7, in which the black solid line represents the measurement without the resonance filters, and the red dashed line represents those performed with the filters. The TOF spectra were normalized by the proton-beam intensity. Based on Fig. 7, two narrow peaks were observed at the beginning of the TOF spectra, which were induced by the γ -flash. The double-peak structure of γ -flash indicates that the accelerator of CSNS operated in the double-bunch mode. The maximum TOF range was 40.0 ms owing to the 25 Hz repetition rate of the pulsed proton beam. The dips absorbed by the ⁵⁹Co, ¹⁸¹Ta, and ^{nat}Ag filters are shown in Fig. 7. The resonance peak of the ⁸¹Br(n, γ)⁸²Br reaction at 135 eV was invisible when

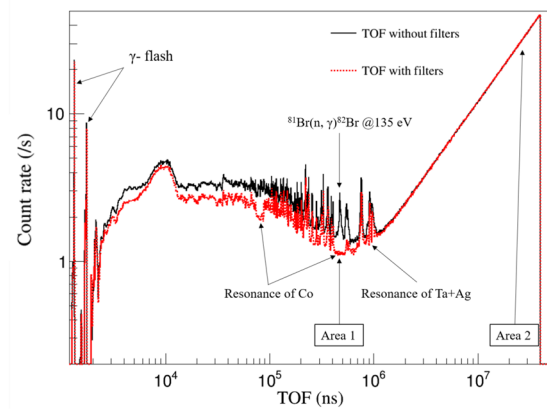


Fig. 7 (Color online) TOF spectra measured with and without the filters: the black solid line represents the TOF without filters, and the red dashed line represents the TOF with filters

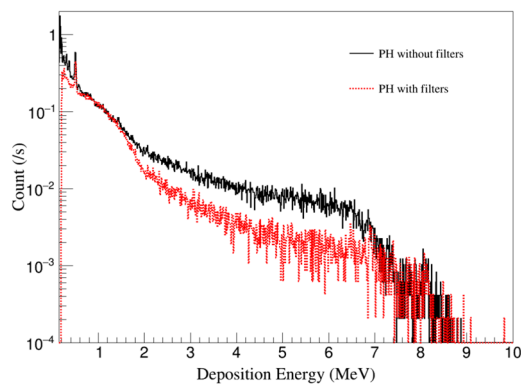


Fig. 8 (Color online) Deposited energy spectra of the CeBr_3 detector in Area 1 with the filters offline (black solid line) and online (red dashed line)

the filters were in place, indicating that the neutrons in this TOF region were completely absorbed by the filters.

4.2 Deposited energy spectrum

The signals in the absorption TOF region between $425 \mu\text{s}$ and $505 \mu\text{s}$ (Area 1) were selected to obtain the deposited energy spectra of the CeBr_3 detector. As shown in Fig. 8, the deposited energy spectrum without the filters (black solid line) was considerably higher than that with the filters (red dashed line) in the energy regions between 1.8 MeV and 7.0 MeV and below 0.511 MeV, which was primarily due to the cascade gamma rays produced by the $^{81}\text{Br}(n,\gamma)^{82}\text{Br}$ reaction around 132 eV.

Ideally, the energy spectrum deposited in the absorption TOF region is mainly attributed to the in-beam gamma rays. However, even in the absorption TOF region, a significant number of gamma rays were from the activation of the environmental materials and the CeBr_3 detector itself. In this study, signals in the TOF region at approximately 28.0 ms (Area 2 in Fig. 7, corresponding to neutron energies less than 0.3 eV) were analyzed to evaluate the contribution of the activation gamma rays. In Area 2, all primary neutrons were absorbed by a ^{nat}Cd filter, and the residual signals were attributed to the activation of gamma rays. Figure 9 shows the normalized deposited energy spectra of Area 1 (black solid line) and Area 2 (red dashed line), indicating that the activation gamma rays mainly affected the energy region below 2.3 MeV. By subtracting the deposited energy spectrum of the activation gamma rays from that of Area 1, the deposited energy spectrum, which was induced only by the in-beam gamma rays, was obtained, as indicated by the blue dotted line in Fig. 9.

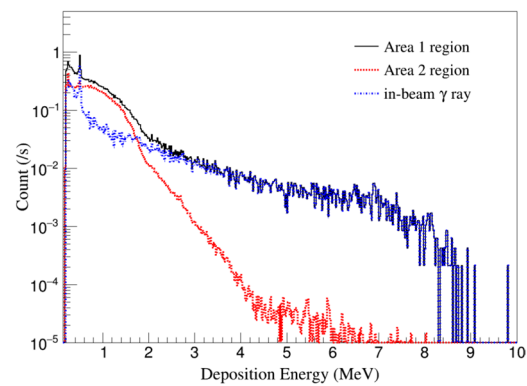


Fig. 9 (Color online) Deposited energy spectra of the in-beam gamma rays, the black solid line is the normalized deposited energy spectrum of Area 1, the red dashed line is the normalized deposited energy spectrum of Area 2, and the blue dotted line indicates the deposited energy spectrum only due to the in-beam gamma rays

5 Results and discussion

5.1 Energy distribution

Using the response function of the CeBr_3 detector for mono-energetic γ rays, the energy distribution of the incident γ rays can be obtained by unfolding the deposited energy spectra using an iterative algorithm. However, the experimental threshold and fluctuation of the deposited energy spectra owing to low statistics make accurately obtaining a real energy distribution over a wide energy range difficult. In this study, a Monte Carlo simulation was utilized to verify the energy distribution of the in-beam gamma rays of Backn. As mentioned in Ref. [14], the entire spallation target was modeled using the Geant4 toolkit, as well as the moderators and reflectors around the target. The time distribution of the in-beam gamma rays was simulated and was in good agreement with the experimental results. The energy spectra of the γ -flash and delayed in-beam gamma rays were obtained using the same simulation. In addition, based on the simulation results, the energy distributions of the delayed in-beam gamma rays were similar for different TOF ranges [14]. Therefore, we propose simulating the response of the CeBr_3 detector to gamma rays with the energy spectrum given by Ref. [14] and comparing the simulated deposited energy spectrum with the experimental one obtained in this study. The entire experimental setup was modeled using the Geant4 toolkit, including the CeBr_3 detector, neutron beamline, BaF_2 detector array [21] installed at the experimental station, beam dump, and walls, as shown in Fig. 10. In addition, resonance filters and neutron-beam windows were included in this simulation.

A circular surface gamma-ray source was constructed using the Geant4 code with a diameter of 20.0 mm, approximately 76 m away from the CeBr_3 detector. The energy of the

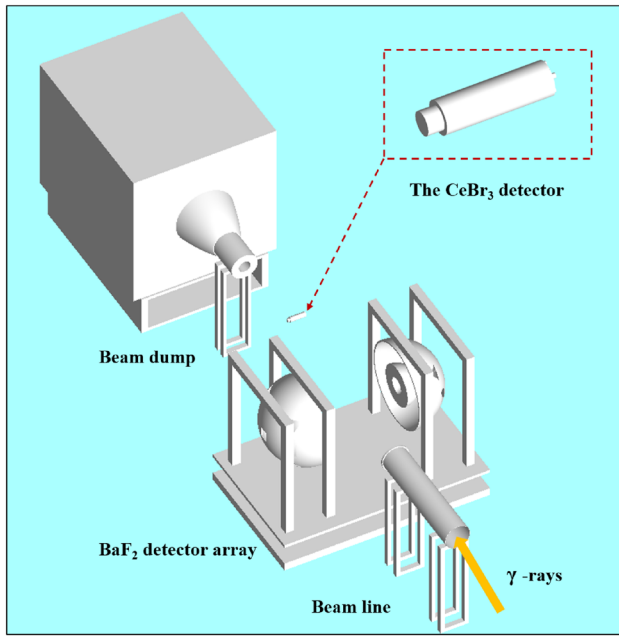


Fig. 10 (Color online) Geometry model of the experimental setup

gamma rays was sampled according to the energy spectrum, as shown in Fig. 11. The peaks at 6 – 10 MeV are associated with gamma rays from the neutron-capture reactions of spallation targets (W, Ta, Fe), and the peak at 2.23 MeV corresponds to gamma rays from the hydrogen capture reactions. Parallel gamma rays passed through the resonance filters in the vacuum beamline. The interactions of gamma rays in the CeBr₃ detector were simulated, and the deposited energy was recorded. The energy resolution function shown in Fig. 5 was used to broaden the simulation spectrum, and a threshold of 150 keV was used in the simulation. Figure 12 shows the simulated deposited energy spectrum, indicated by the red dashed line, and the black solid line represents the experimental result corresponding to the blue dotted line in

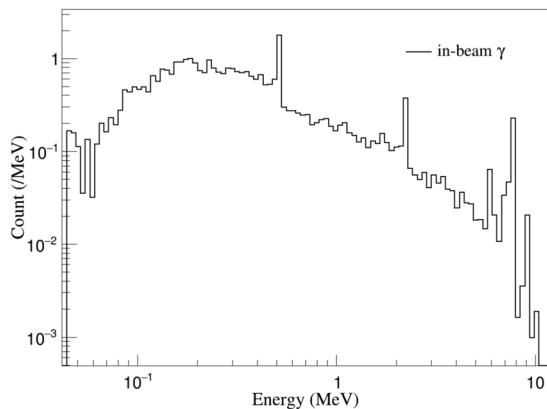


Fig. 11 Energy distribution of the delayed in-beam gamma rays

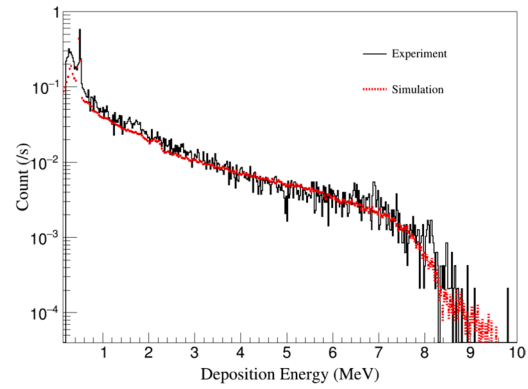


Fig. 12 (Color online) Comparison between the measured deposited energy spectrum of the in-beam gamma rays in the CeBr₃ detector and the simulated spectrum

Fig. 9. According to Fig. 12, the simulated deposited energy spectrum is consistent with the experimental spectrum above 0.4 MeV, indicating that the energy distribution used in this simulation can reasonably reflect the real energy spectra of the in-beam gamma rays at Back-n.

5.2 Flux calculation

Using the energy distribution of the in-beam gamma rays and the detection efficiency of the CeBr₃ detector, the flux (Φ_γ) was obtained in the work via the following relation:

$$\Phi_\gamma = f \cdot \frac{N}{S \cdot \epsilon}, \tag{3}$$

where N is the count rate of the measured deposited energy spectrum in the energy region between 0.4 MeV and 10 MeV in Fig. 12, with the units being events per second. S is the effective area of the CeBr₃ detector covered by the in-beam gamma rays, with units of square centimeters. ϵ is the detection efficiency of the CeBr₃ detector, and f is the correction factor, with no units.

In the present measurement, the count rate N was 0.73 ± 0.03 per second. The uncertainty was mainly due to the poor statistics of gamma rays with deposited energies above 7 MeV and the uncertainty of the threshold. The effective area S was 1.57 cm^2 , which was equal to half the area of the beam spot, as recommended by Ref. [9]. According to the measurement results of the beam spot at Back-n [34], the measured diameter of the beam spot in ES#2 is $\sim 5\%$ larger than the simulated diameter. Therefore, the uncertainty of S was assigned a value of 7.07% in this study. In this study, ϵ was determined via Monte Carlo simulations because no gamma-ray source had the same energy distribution as the in-beam gamma rays for the detection efficiency calibration. The gamma-ray generator and detector geometry were the same as those mentioned in Sect. 5.1 in the Geant4 code. In

addition, a resolution function was considered and a threshold of 0.4 MeV was used in this simulation. In this study, the detection efficiency was calculated to be 0.29. Determining the uncertainty of ϵ was difficult because it was the total simulation result. The statistical uncertainty was less than 0.1% in the simulation. The uncertainty owing to the standard electromagnetic physics model used in the Geant4 toolkit in the energy region below 10.0 MeV was assumed to be 2.0%. The uncertainty of ϵ was mainly due to the energy distribution of the in-beam gamma rays used in the simulation. A conservative value of 10.0% was assigned to the uncertainty in the energy distribution of the in-beam gamma rays. Therefore, the uncertainty of ϵ was $\sim 10.20\%$.

The correction factor f in Eq. (3) can be expressed as follows:

$$f = f_{\text{att}} \cdot f_{\text{tof}} \cdot f_{\text{dt}}, \quad (4)$$

where f_{att} is the correction factor for the attenuation of gamma rays passing through the black resonance filters. f_{tof} represents the ratio of the total flux of in-beam gamma rays to the flux of gamma rays within a specific absorption region of the TOF spectrum. f_{dt} is the dead-time correction factor, which is due to the pileup of signals when the counting rate is high.

The attenuation factor f_{att} was calculated using the Geant4 toolkit. The simulation procedure was similar to that used to calculate the detection efficiency. f_{att} was determined by simulating the ratio between the detector responses to the in-beam gamma rays with and without the resonance filters in the flight path. Considering the resolution function and detection threshold, the attenuation factor f_{att} was equal to 1.55 in this study. The uncertainty of f_{att} was assigned a conservative value of 2.0%.

f_{tof} was used in this study because only the absorption region in the TOF spectrum was used to measure the in-beam gamma rays, whereas the in-beam gamma rays lasted for more than 2 ms after the proton beam was injected into the spallation target. According to the time distribution given in Ref. [14], the total number of in-beam gamma rays was 1.0 after normalization, whereas the integral count of gamma rays with a TOF between 425 μs and 505 μs was 6.76×10^{-4} . f_{tof} was equal to 1.48×10^3 in this calculation. In Ref. [14], the time distribution of in-beam gamma rays was simulated and verified using experimental data. Therefore, the uncertainty of f_{tof} was estimated to be less than 10.0%.

The dead-time correction factor f_{dt} was determined as follows:

$$f_{\text{dt}} = \frac{1}{1 - \tau N_i}, \quad (5)$$

where τ is the time interval used in the waveform analysis, in which all signals that occurred were treated as one signal pulse and N_i is the counting rate associated with a bin in the TOF spectrum. In this study, τ was set to 60 ns to process the waveforms after the fast-filter procedure. Figure 13 shows the f_{dt} obtained from the measurement with a 3 – 15 – 40 mm collimator assignment, where the presence of filters is indicated by the black solid line, and their absence by the red dashed line. Based on Fig. 13, the dead-time correction factor f_{dt} around the absorption region (Area 1) was 1.0 ± 0.001 ; thus, very few pileup signals were observed under this experimental condition.

Using Eq. (3), the flux of the in-beam gamma rays measured by the CeBr₃ detector with a 3 – 15 – 40 mm collimator assignment was $3.68\text{e}3 \text{ cm}^{-2} \text{ s}^{-1}$. The values of the parameters in Eq. (3), Eq. (4) and their uncertainties are listed in Table 2.

Three types of collimator assignments were used in the measurements: 3 – 15 – 40 mm, 12 – 15 – 40 mm, and 50 – 15 – 40 mm. Figure 14 shows the TOF spectrum with different collimator assignments and with the resonance filters online. As the aperture of the first collimator increased, the response of the CeBr₃ detector became significantly delayed. This was because the flux of the γ -flash became considerably stronger, such that the CeBr₃ detector was blinded and the recovery time was typically greater than 20 μs . Notably, the threshold used in the measurements for Fig. 14 was approximately 2.0 MeV. This occurred because when the aperture of the first collimator was larger than 3 mm, the data size with a low threshold was considerably larger than the data-transmission limit, which was 5.12 MB/s for the DT5730B. Considering that the flux of the in-beam gamma rays with the 3 – 15 – 40 mm collimator assignment ($\Phi_{\gamma,3-15-40}$) was measured previously, the flux of the other collimator assignments could be determined via

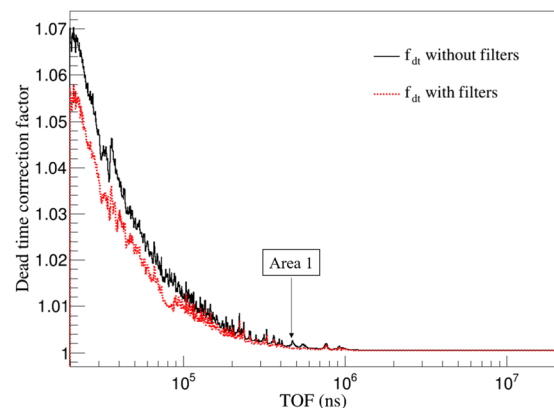


Fig. 13 (Color online) Dead-time correction factor of the measurement with 3 – 15 – 40 mm collimator assignment

Table 2 Parameters were used for the flux calculation

Parameters	N (s ⁻¹)	S (cm ⁻²)	ϵ	f_{att}	f_{tof}	f_{dt}
Value	0.73	1.57	0.29	1.55	1.48e ³	1.0
Uncertainty (%)	4.11	7.07	10.2	2.0	10.0	0.1

Table 3 Flux of the in-beam gamma rays

Collimator (mm)	Flux (cm ⁻² s ⁻¹)	Uncertainty (%)
3–15–40	3.68e3	16.58
12–15–40	3.16e4	18.06
50–15–40	3.6e5	18.74

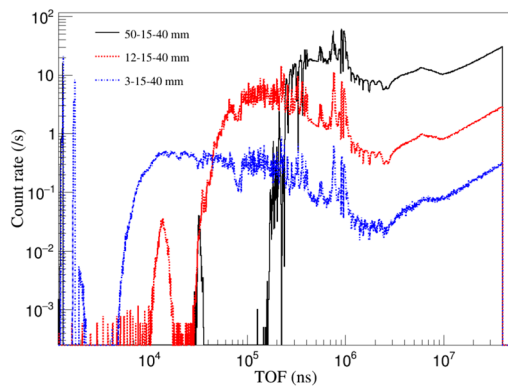


Fig. 14 (Color online) TOF spectra of the measurement with different collimator assignments, black (solid) for 50 – 15 – 40 mm, red (dashed) for 12 – 15 – 40 mm, and blue (dotted) for 3 – 15 – 40 mm

$$\Phi_{\gamma} = \frac{N}{N_{3-15-40}} \cdot \frac{S_{3-15-40}}{S} \cdot \Phi_{\gamma,3-15-40} \tag{6}$$

where N is the count rate of the TOF spectra in the region between 425 μs and 505 μs and S is the effective area, as shown in Eq. (3). For collimator assignments of 12 – 15 – 40 mm and 50 – 15 – 40 mm, the S values were 3.53 cm² according to Ref. [9]. The flux of the in-beam gamma rays, calculated using Eq. (6), is listed in Table 3. The uncertainties were mainly due to the measurement statistics, uncertainty of the effective area, uncertainty of the dead-time correction, and uncertainty of $\Phi_{\gamma,3-15-40}$. The uncertainties of the flux in Table 3 were 16.58 % for $\Phi_{\gamma,3-15-40}$, 18.06 % for $\Phi_{\gamma,12-15-40}$, and 18.74 % for $\Phi_{\gamma,50-15-40}$.

Based on the energy distribution shown in Fig. 11 and the total flux of the in-beam gamma rays, the flux of the delayed in-beam gamma rays at ES#2 of Back-n was determined in different energy regions. The determined fluxes are listed in Table 4.

Table 4 Flux of delayed in-beam gamma rays at ES#2 of Back-n in different energy ranges

Energy (MeV)	Flux (3–15–40) (cm ⁻² s ⁻¹)	Flux (12–15–40) (cm ⁻² s ⁻¹)	Flux (50–15–40) (cm ⁻² s ⁻¹)
Below 0.4	913.65	7845.46	90620.01
0.4–1.0	833.04	7153.29	82625.05
1.0–2.0	540.80	4643.84	53639.31
2.0–3.0	389.52	3344.80	38634.52
3.0–4.0	179.87	1544.54	17840.43
4.0–5.0	104.83	900.13	10397.06
5.0–6.0	95.69	821.71	9491.28
6.0–7.0	113.16	971.73	11224.12
7.0–8.0	455.04	3907.37	45132.62
8.0–9.0	14.29	122.74	1417.78
9.0–12.0	40.10	344.37	3977.66

5.3 Background evaluation for (n,γ) reaction measurement

By utilizing the energy distribution and flux of the in-beam gamma rays determined in this study, the experimental background induced by the in-beam gamma rays can be evaluated for neutron-reaction measurements at Back-n, which is helpful for experimental optimization and data analysis. Taking the radiative neutron-capture cross-section measurement using the C₆D₆ detectors at Back-n as an example, the gamma rays detected by the C₆D₆ detectors may originate from (n,γ) reactions or from the interactions of the in-beam gamma rays with the experimental sample. The C₆D₆ detector cannot distinguish between the in-beam gamma rays scattered off the sample and those produced by the neutron-capture reaction. Therefore, the experimental background increased with an increase in the number of scattered in-beam gamma rays.

To study the effect and background before an actual measurement, we propose simulating the response of the C₆D₆ detectors to in-beam gamma rays, as well as gamma rays from the (n,γ) reaction.

geometrical model of the C₆D₆ detectors was built with the Geant4 toolkit, similar to the model used in Ref. [10]. Two samples, ¹⁹⁷Au and ²⁰⁹Bi, were selected for the simulation in this study, with diameters of 30.0 mm and 1.0 mm respectively. The scattered cross sections of ¹⁹⁷Au and ²⁰⁹Bi for the gamma rays were similar, whereas the neutron-capture cross section of ¹⁹⁷Au was significantly larger than that

of ^{209}Bi . In this simulation, neutrons and gamma rays were generated approximately 76 m away from the ^{197}Au and ^{209}Bi samples, which was the same as the distance between the experimental sample and spallation target of CSNS. The energy distribution and flux of the neutron beam of Back-n used in the simulation were obtained from Ref. [8], and the time distribution of the in-beam gamma rays was obtained from Ref. [14]. Because the collimator assignment used in the radiative neutron-capture cross-section measurement was typically 12 – 50 – 40 mm, the fluxes of the neutron beam and in-beam gamma rays were given as $7.81 \times 10^5 \text{ cm}^{-2} \text{ s}^{-1}$ [9] and $3.16 \times 10^4 \text{ cm}^{-2} \text{ s}^{-1}$, respectively. The TOF spectra of the responses of the C_6D_6 detectors to scattered in-beam gamma rays (black solid line) and gamma rays from the (n,γ) reaction (red dashed line) are shown in Fig. 15. Figure 15a shows the simulated result of the ^{197}Au sample, while Fig. 15b shows that of the ^{209}Bi sample. The time structure of the proton-beam pulse and time resolution of the neutron beam of Back-n were not involved in the TOF spectra. According to the TOF spectra, the γ -flash scattered off the sample at approximately 230 ns, causing a significant

response in the C_6D_6 detector. Subsequently, the detector's response to the in-beam gamma rays persisted for approximately 4.5 ms. Only (n,γ) reactions induced by neutrons with energies between 0.3 eV and 20.0 MeV were recorded in the simulation. Therefore, the TOF for the reaction gamma rays was primarily within the range of approximately 1 μs to 10 ms. The signal-to-background ratio of Fig. 15a was better than that of Fig. 15b because the cross section of $^{197}\text{Au}(n,\gamma)^{198}\text{Au}$ was approximately ten to a hundred times larger than that of the $^{209}\text{Bi}(n,\gamma)^{210}\text{Bi}$ reaction. The poor signal-to-background ratio shown in Fig. 15b indicates that determining the cross section of the $^{209}\text{Bi}(n,\gamma)^{210}\text{Bi}$ reaction when using the C_6D_6 detector at Back-n requires the precise removal of this background. This simulation provided a preliminary evaluation of the background induced by in-beam gamma rays in neutron-capture cross-sectional measurements. However, the pulse-height weighting technique, neutron-scattering background, and activation background were not considered in this simulation. To determine the in-beam gamma background accurately, dedicated measurements of the Pb and C samples should be performed in the neutron-capture cross section measurement at Back-n [14–25].

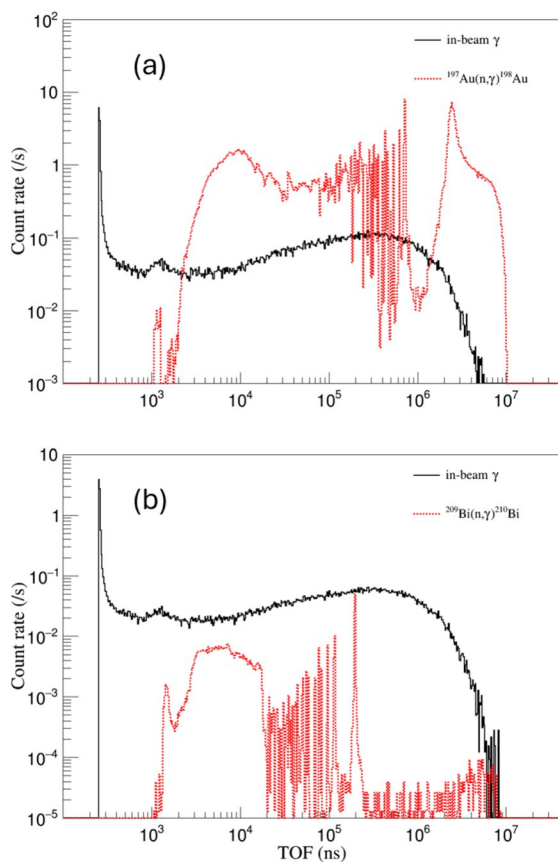


Fig. 15 (Color online) Simulated TOF spectra of the responses of the C_6D_6 detectors to the scattered in-beam gamma rays (black solid line) and gamma rays from the (n,γ) reaction (red dashed line) of the (a) ^{197}Au sample and (b) ^{209}Bi sample

6 Conclusion

In-beam gamma rays are common in almost all spallation neutron facilities and may affect the detectors on the beam-line and increase the experimental background. In this study, the energy distribution of the in-beam gamma rays of Back-n was verified using the black resonance filter method and analyzed using Monte Carlo simulations. In addition, the flux of the in-beam gamma rays was determined. With the characteristics of in-beam gamma rays, the feasibility of neutron-reaction measurements at Back-n could be reasonably evaluated before an actual experiment.

According to the results of this measurement, the energy of the in-beam gamma rays ranged from keV to approximately 10 MeV, with approximately 75 % above 0.4 MeV. Most high-energy in-beam gamma rays after the γ -flash are produced by neutron-capture reactions in the spallation target. Three collimator assignments were used in this study, and the fluxes of the in-beam gamma rays with different collimator apertures were more than 10 times lower than the neutron fluxes with the same collimator assignment, according to Ref. [8]. Considering that more than 90 % of the in-beam gamma rays are γ -flash rays, the flux of the delayed in-beam gamma rays, which may affect the (n,γ) cross section measurement, was more than 100 times lower than that of the neutron beam. However, for an isotope with a small (n,γ) reaction cross section and high gamma scattering cross section, the background induced by the in-beam gamma rays was still too high to perform an accurate measurement with

a C_6D_6 detector system. Therefore, we recommend using the $4\pi BaF_2$ array detection system to measure the (n,γ) reaction with a small cross section at Back-n. By measuring the multiplicity and total energy of the (n,γ) reaction, the background due to scattered in-beam gamma rays can be effectively suppressed, and the accuracy of the measurement can be significantly improved.

Acknowledgements The authors are indebted to the operating crew of the CSNS Back-n white-neutron source.

Author's contribution All authors contributed to the study conception and design. Material preparation, data collection, and analysis were performed by J-CW, JR, X-CR, WJ, C, Y-YL, H-LY, K-ZX, X-YP, QS, JB, H-XH, H-FB, J-BB, PC, Q-PC, Y-HC, W-HD A-CF, R-RF, C-QF, M-HG, C-CH, Z-JH, G-ZH, Y-CH, YH, Y-WH, Z-JJ, LK, C-LL, BL, FL, QL, XL, YL, JL, RL, S-BL, Y-NL, G-YL, C-JN, Y-jQ, W-KR, Z-ZR, Z-HS, KS, Z-XT, J-YT, S-D T, L-JW, P-CW, Z-HW, Z-WW, X-GW, XW, Z-PW, CX, L-KX, HY, TY, Y-JY, G-HZ, H-CZ, Q-WZ, X-PZ, Y-LZ, Z-YZ, M-YZ, Z-HZ, K-JZ, and CZ. The first draft of the manuscript was written by Jin-Cheng Wang, and all authors commented on previous versions of the manuscript. All authors read and approved the final manuscript.

Data availability The data that support the findings of this study are openly available in Science Data Bank at <https://cstr.cn/31253.11.sciencedb.j00186.00223> and <https://www.doi.org/10.57760/sciencedb.j00186.00223>.

Declarations

Conflict of interest Jing-Yu Tang and Ke-Jun Zhu are the editorial board members for Nuclear Science and Techniques and were not involved in the editorial review, or the decision to publish this article. All authors declare that there is no conflict of interest.

References

- H.S. Chen, X.L. Wang, China's first pulsed neutron source. *Nat. Mater.* **15**(7), 689–691 (2016). <https://doi.org/10.1038/nmat4655>
- M.Y. Huang, J.X. Chen, C.D. Deng et al., Study on the important technologies of 300 MeV upgrade for the CSNS injection system. 12th International Particle Accelerator Conference, (2021). <https://doi.org/10.18429/JACoW-IPAC2021-WEPAB199>
- X.F. Jiang, J.R. Zhou, H. Luo et al., A large area 3He tube array detector with vacuum operation capacity for the SANS instrument at the CSNS. *Nucl. Sci. Tech.* **33**, 89 (2022). <https://doi.org/10.1007/s41365-022-01067-1>
- H.T. Jing, J.Y. Tang, H.Q. Tang et al., Studies of back-streaming white neutrons at CSNS. *Nucl. Instrum. Meth. A* **621**(1), 91–96 (2010). <https://doi.org/10.1016/j.nima.2010.06.097>
- L. Zhu, J.R. Zhou, Y.G. Xia et al., Large area 3He tube array detector with modular design for multi-physics instrument at CSNS. *Nucl. Sci. Tech.* **34**, 1 (2023). <https://doi.org/10.1007/s41365-022-01161-4>
- Y.C. He, S.W. Xiao, G.Y. Wang et al., Prototype motion control system for CSNS very small angle neutron scattering instrument. *Nucl. Tech.* (in Chinese) **45**(8), 080401 (2022). <https://doi.org/10.11889/j.0253-3219.2022.hjs.45.080401>
- J.Y. Tang, F.S. Nian, H.T. Jing et al., Proposal for muon and white neutron sources at CSNS. *Chin. Phys. C* **34**(1), 121 (2010). <https://doi.org/10.1088/1674-1137/34/1/022>
- Y.H. Chen, G.Y. Luan, J. Bao et al., Neutron energy spectrum measurement of the Back-n white neutron source at CSNS. *Eur. Phys. J. A* **55**(7), 115 (2019). <https://doi.org/10.1140/epja/i2019-12808-1>
- Q. An, H.Y. Bai, J. Bao, P. Cao et al., Back-n white neutron facility for nuclear data measurements at CSNS. *J. Instrum.* **12**(7), P07022 (2017). <https://doi.org/10.1088/1748-0221/12/07/P07022>
- J. Ren, X.C. Ruan, J. Bao et al., The $C_6 D_6$ detector system on the Back-n beam line of CSNS. *Radiat. Detect. Technol. Methods* **3**, 52 (2019). <https://doi.org/10.1007/s41605-019-0129-8>
- L.Y. Zhang, H.T. Jing, J.Y. Tang et al., Design of back-streaming white neutron beam line at CSNS. *Appl. Radiat. Isotopes* **132**, 212–221 (2018). <https://doi.org/10.1016/j.apradiso.2017.11.013>
- Q. Li, G.Y. Luan, J. Bao et al., The 6LiF -silicon detector array developed for real-time neutron monitoring at white neutron beam at CSNS. *Nucl. Instrum. Meth. A* **946**, 162497 (2019). <https://doi.org/10.1016/j.nima.2019.162497>
- X.Y. Liu, Y.W. Yang, R. Liu et al., Measurement of the neutron total cross section of carbon at the Back-n white neutron beam of CSNS. *Nucl. Sci. Tech.* **30**(9), 139 (2019). <https://doi.org/10.1007/s41365-019-0660-9>
- J. Ren, X.C. Ruan, J. Bao, G.Y. Luan et al., In-beam gamma-rays of back-streaming white neutron source at china spallation neutron source. *Acta. Phys. Sin.* **69**(17), 9 (2020). <https://doi.org/10.7498/aps.69.20200718>
- J. Ren, X.C. Ruan, W. Jiang et al., Neutron capture cross section of ^{169}Tm measured at the CSNS Back-n facility in the energy region from 30 to 300 keV*. *Chin. Phys. C* **46**(4), 044002 (2022). <https://doi.org/10.1088/1674-1137/ac4589>
- X.R. Hu, L.X. Liu, W. Jiang et al., New experimental measurement of $^{nat}Se(n,\gamma)$ cross section between 1 eV to 1 keV at the CSNS Back-n facility. *Chin. Phys. B* **31**(8), 080101 (2022). <https://doi.org/10.1088/1674-1056/ac6ee2>
- X.X. Li, L.X. Liu, W. Jiang et al., Measurements of the ^{107}Ag neutron capture cross sections with pulse height weighting technique at the CSNS Back-n facility. *Chin. Phys. B* **31**(3), 038204 (2022). <https://doi.org/10.1088/1674-1056/ac48fd>
- B. Jiang, J.L. Han, J. Ren et al., Measurement of $^{232}Th(n,\gamma)$ cross section at the CSNS Back-n facility in the unresolved resonance region from 4 keV to 100 keV. *Chin. Phys. B* **31**(6), 060101 (2022). <https://doi.org/10.1088/1674-1056/ac5394>
- J. Ren, X.C. Ruan, J. Bao et al., Introduction of a $C_6 D_6$ detector system on the Back-n of CSNS. *EPJ Web. Conf.* **239**, 17021 (2020). <https://doi.org/10.1051/epjconf/202023917021>
- J. Ren, X.C. Ruan, W. Jiang et al., Background study for (n,γ) cross section measurements with $C_6 D_6$ detectors at CSNS Back-n. *Nucl. Instrum. Meth. A* **985**, 164703 (2021). <https://doi.org/10.1016/j.nima.2020.164703>
- Q.W. Zhang, G.Y. Luan, J. Ren et al., Cross section measurement of neutron capture reaction based on back-streaming white neutron source at China spallation neutron source. *Acta. Phys. Sin.* **70**, 222801 (2021). <https://doi.org/10.7498/aps.70.20210742>
- Z.D. An, W.W. Qiu, W. Jiang et al., Measurement of the $^{181}Ta(n,\gamma)$ cross sections up to stellar s-process temperatures at the CSNS Back-n. *Sci. Rep-uk* **13**, 12657 (2023). <https://doi.org/10.1038/s41598-023-39603-7>
- S. Zhang, G. Li, W. Jiang et al., Measurement of the $^{159}Tb(n,\gamma)$ cross section at the CSNS Back-n facility. *Phys. Rev. C* **107**, 045809 (2023). <https://doi.org/10.1103/PhysRevC.107.045809>
- J.C. Wang, J. Ren, W. Jiang et al., Determination of the $^{232}Th(n,\gamma)$ cross section from 10 to 200 keV at the Back-n facility at CSNS. *Eur. Phys. J. A* **59**, 224 (2023). <https://doi.org/10.1140/epja/s10050-023-01126-0>
- X.X. Li, L.X. Liu, W. Jiang et al., Experimental determination of the neutron resonance peak of ^{162}Er at 67.8 eV. *Phys. Rev. C* **106**, 065804 (2022). <https://doi.org/10.1103/PhysRevC.106.065804>

26. Y.H. Chen, Y.W. Yang, Z.Z. Ren et al., Measurement of neutron-induced fission cross sections of ^{232}Th from 1 to 300 MeV at CSNS Back-n. *Phys. Lett. B* **839**, 137832 (2023). <https://doi.org/10.1016/j.physletb.2023.137832>
27. Y.J. Qiu, C.L. Lan, Y.H. Chen et al., Measurement of the $^{239}\text{Pu}(n,f)$ cross section from 4 keV to 00 MeV using the white neutron source at the CSNS Back-n facility. *Phys. Rev. C* **107**, 024606 (2023). <https://doi.org/10.1103/PhysRevC.107.024606>
28. H.Y. Bai, R.R. Fan, H.Y. Jiang et al., Measurement of the differential cross sections and angle-integrated cross sections of the $^6\text{Li}(n,t)^4\text{He}$ reaction from 1.0 eV to 3.0 MeV at the CSNS Back-n white neutron source *. *Chin. Phys. C* **44**, 014003 (2020). <https://doi.org/10.1088/1674-1137/44/1/014003>
29. H.Y. Jiang, W. Jiang, H.Y. Bai et al., Measurements of differential and angle-integrated cross sections for the $^{10}\text{B}(n,\alpha)^7\text{Li}$ reaction in the neutron energy range from 1.0 eV to 2.5 MeV*. *Chin. Phys. C* **43**, 124002 (2019). <https://doi.org/10.1088/1674-1137/43/12/124002>
30. D.B. Syme, The black and white filter method for background determination in neutron time-of-flight spectrometry. *Nucl. Instrum. Meth.* **198**(2), 357–364 (1982). [https://doi.org/10.1016/0167-5087\(82\)90276-9](https://doi.org/10.1016/0167-5087(82)90276-9)
31. J. Allison, K. Amako, J. Apostolakis et al., Recent developments in GEANT4. *Nucl. Instrum. Meth. A* **835**, 186–225 (2016). <https://doi.org/10.1016/j.nima.2016.06.125>
32. K.S. Shah, J. Glodo, W. Higgins et al., CeBr_3 scintillators for gamma-ray spectroscopy. *IEEE. T. Nucl. Sci* **52**(6), 3157–3159 (2005). <https://doi.org/10.1109/TNS.2005.860155>
33. F.G.A. Quarati, P. Dorenbos, J. Van Der Biezen et al., Scintillation and detection characteristics of high-sensitivity CeBr_3 gamma-ray spectrometers. *Nucl. Instrum. Meth. A* **729**, 596–604 (2013). <https://doi.org/10.1016/j.nima.2013.08.005>
34. X.P. Zhang, G.Y. Luan, J. Ren et al., Experimental result of back-streaming white neutron beam characterization at Chinese spallation neutron source. *Acta. Phys. Sin.* **68**(8), 080101 (2019). <https://doi.org/10.7498/aps.68.20182191>

Springer Nature or its licensor (e.g. a society or other partner) holds exclusive rights to this article under a publishing agreement with the author(s) or other rightsholder(s); author self-archiving of the accepted manuscript version of this article is solely governed by the terms of such publishing agreement and applicable law.

Authors and Affiliations

Jin-Cheng Wang¹ · Jie Ren¹ · Wei Jiang^{2,3} · Xi-Chao Ruan¹ · Ying-Yi Liu¹ · Hao-Lan Yang¹ · Kuo-Zhi Xu¹ · Xin-Yi Pan¹ · Qi Sun¹ · Jie Bao¹ · Han-Xiong Huang¹ · Hao-Fan Bai⁴ · Jiang-Bo Bai⁵ · Ping Cao^{6,7} · Qi-Ping Chen⁸ · Yong-Hao Chen^{2,3} · Wen-Hao Duan^{6,9} · An-Chuan Fan¹⁰ · Rui-Rui Fan^{2,3,11} · Chang-Qing Feng^{6,9} · Min-Hao Gu^{2,11} · Chang-Cai Han¹² · Zi-Jie Han⁸ · Guo-Zhu He¹ · Yong-Cheng He^{2,3} · Yang Hong^{2,3,13} · Yi-Wei Hu⁴ · Zhi-Jie Jiang^{6,9} · Ling Kang^{2,3} · Chang-Lin Lan¹⁴ · Bo Li^{2,3} · Feng Li^{6,9} · Qiang Li^{2,3} · Xiao Li^{2,3} · Yang Li^{2,3} · Jie Liu⁴ · Rong Liu⁸ · Shu-Bin Liu^{6,9} · Yi-Na Liu¹ · Guang-Yuan Luan¹ · Chang-Jun Ning^{2,3} · Yi-Jia Qiu^{2,3} · Wen-Kai Ren⁴ · Zhi-Zhou Ren⁸ · Zhao-Hui Song¹² · Kang Sun^{2,3,13} · Zhi-Xin Tan^{2,3} · Jing-Yu Tang^{6,7} · Sheng-Da Tang^{2,3} · Li-Jiao Wang^{2,3,13} · Peng-Cheng Wang^{2,3} · Zhao-Hui Wang¹ · Zhong-Wei Wen⁸ · Xiao-Guang Wu¹ · Xuan Wu^{2,3} · Ze-Peng Wu⁴ · Cong Xia⁴ · Li-Kun Xie¹⁵ · Han Yi^{2,3} · Tao Yu¹⁵ · Yong-Ji Yu^{2,3} · Guo-Hui Zhang⁴ · Hang-Chang Zhang² · Qi-Wei Zhang¹ · Xian-Peng Zhang¹² · Yu-Liang Zhang^{2,3} · Zhi-Yong Zhang^{6,9} · Mao-Yuan Zhao^{6,9} · Zhi-Hao Zhou^{2,3,13} · Ke-Jun Zhu^{2,11,13} · Chong Zou¹

✉ Jie Ren
renjie@ciae.ac.cn

✉ Xi-Chao Ruan
xichao_ruan@126.com

- ¹ Key Laboratory of Nuclear Data, China Institute of Atomic Energy, Beijing 102413, China
- ² Institute of High Energy Physics, Chinese Academy of Sciences (CAS), Beijing 100049, China
- ³ Spallation Neutron Source Science Center, Dongguan 523803, China
- ⁴ State Key Laboratory of Nuclear Physics and Technology, School of Physics, Peking University, Beijing 100871, China
- ⁵ Institute of Modern Physics, Fudan University, Shanghai 200433, China
- ⁶ State Key Laboratory of Particle Detection and Electronics, University of Science and Technology of China, Hefei 230026, China
- ⁷ School of Nuclear Science and Technology, University of Science and Technology of China, Hefei 230026, China

⁸ Institute of Nuclear Physics and Chemistry, China Academy of Engineering Physics, Mianyang 621900, China

⁹ Department of Modern Physics, University of Science and Technology of China, Hefei 230026, China

¹⁰ USTC Archaeometry Lab, University of Science and Technology of China, Hefei 230026, China

¹¹ State Key Laboratory of Particle Detection and Electronics, Institute of High Energy Physics Chinese Academy of Sciences, Beijing 100049, China

¹² Northwest Institute of Nuclear Technology, Xi'an 710024, China

¹³ University of Chinese Academy of Sciences, Beijing 100049, China

¹⁴ School of Nuclear Science and Technology, Lanzhou University, Lanzhou 730000, China

¹⁵ Institute of Advanced Technology, University of Science and Technology of China, Hefei 230027, China